AIAA JOURNAL
Vol. 30, No. 2, February 1992

Experiments on Active Control of Vibrational Power Flow Using Piezoceramic Actuators/Sensors

Gary P. Gibbs* and Chris R. Fuller†
Virginia Polytechnic Institute and State University, Blacksburg, Virginia 24061

The active control of flexural power flow in both semi-infinite and finite elastic beams is experimentally investigated. The experimental results demonstrate that piezoceramic transducers, when used in conjunction with an adaptive least mean squares narrow-band controller, can effectively control flexural power flow at steady-state single frequencies in thin beam systems. The piezoceramic transducers offer distinct size and weight advantages over conventional transducers. The experiments also demonstrate the use of an axial scanning laser vibrometer to determine out-of-plane velocity and power flow.

Introduction

CONTROL of structure-borne noise is an important problem in many aerospace and marine environments. Various passive techniques have traditionally been used to reduce this unwanted structure-borne noise. However, passive techniques are difficult to apply in situations where the source characteristics are changing and it is in this situation that active control approaches have shown much promise. In particular, work by Redman-White et al.,[1] von Flotow and Schafer,[2] and Gonidou and Fuller[3] has demonstrated that active forces applied to beam-like structures can attenuate bending waves and associated flexural power flow in the media. Reference 4 showed that flexural power flow leaving finite beams terminated by an impedance (representative of a structural joint) could be controlled with only one control input.[4] This is in contrast to the normal modal approach of trying to reduce the total vibrational energy of the section.[5] Thus, if vibrational energy from machinery can be confined to the immediate supporting structure before dispersing through the overall system, then efficient control approaches can be implemented. Although point force actuators give high attenuation rates, they have a number of disadvantages; they are generally obtrusive, require back reaction supports, and can consume high power.

It is the purpose of this paper to demonstrate the effectiveness of piezoceramic actuators and sensors in controlling flexural velocity and power flow in elastic beams. In contrast to point force actuators, piezoelectric actuators (piezoceramic or PVDF) can be bonded or embedded in the beams and are thus unobtrusive and require no support structures. They are also cheap and usually consume low power. However, one question that needs to be addressed with such transducers is the degree of control authority they can exert. Early work by Crawley and deLuis[6] has demonstrated that piezoceramic elements bonded to the beam surface show much potential for excitation of structures. More recently, Pines and von Flotow[7] and Gibbs and Fuller[8] have shown that piezoceramic elements can be used as both actuators and sensors in the control of vibration and power flow in beams. As shown by Crawley and deLuis,[6] a piezoceramic actuator, when bonded to the surface of the beam, effectively induces a surface strain due to its contraction and expansion when excited by an oscillating voltage. Being offset from the neutral axis of the beam, the actuator also causes bending of the structure. In these series of experiments, the elements are bonded symmetrically on each side of the beam and are driven 180 deg out of phase. This has the effect of inducing bending motion in the structure (by symmetry).

Experimental Arrangement

A schematic for the test arrangement used in the following experiments is presented in Fig. 1. The beam is made of aluminum and has the dimensions of 4 m × 32.8 mm × 7.6 mm. The beam is fitted at one end with an anechoic termination that has been tested to have a power reflection coefficient of <0.1 for frequencies above 150 Hz.

The primary source (noise source) is applied as a point force at the free end perpendicular to the surface of the beam. In order to provide control input to the beam, two piezoceramic elements were bonded symmetrically to the beam at a distance of 0.4 m from the free end. These elements were made of lead zirconate titante material and had the dimensions 38.1 × 22.2 × 0.19 mm and were hard wired 180 deg out of phase to induce a bending moment on the beam. The actuator configuration as well as the form of induced strain distribution for thin actuators is shown in Fig. 2.

Two similar transducers were bonded 2.15 m from the free end and were used as the flexural wave error sensors. When these sensors are wired so that their outputs are summed 180 deg out of phase, they produce an oscillating signal that is proportional to the response of the flexural wave motion.

In order to have independent verification of the control of the flexural wave and measure the flexural power flow distribution along the beam, an axial scanning laser vibrometer was used to measure out-of-plane velocity. Using cross-spectral information from two separate velocity measurements (lo-

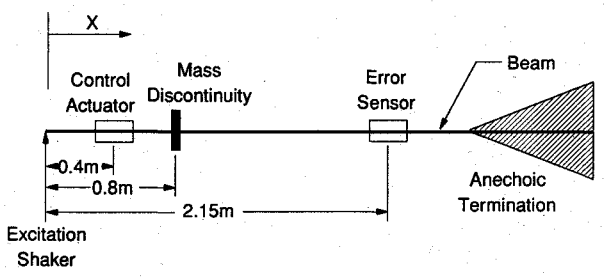

Fig. 1 Experimental schematic.

Presented as Paper 90-1132 at the AIAA/ASME/ASCE/AHS/ASC 31st Structures, Structural Dynamics, and Materials Conference, Long Beach, CA, April 2–4, 1990; received June 29, 1990; revision received Feb. 1, 1991; accepted for publication Feb. 7, 1991.

*Research Associate, Department of Mechanical Engineering. Member AIAA.
†Professor, Department of Mechanical Engineering. Member AIAA.

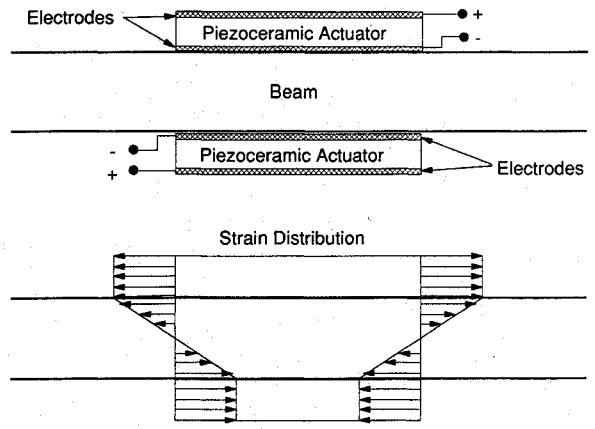

Fig. 2 Piezoceramic transducer.

cated away from discontinuity near fields), the net flexural power flow was calculated as outlined in the Appendix.

Control Implementation

A schematic of the adaptive control system is shown in Fig. 3. The control system uses an adaptive Filtered-X least mean squares (LMS) technique[9] to adapt the coefficients of a finite impulse response (FIR) control filter based on reference and error signals. The control algorithm was implemented using a TMS 320C25 signal processing chip with an IBM AT as a host computer. The sampling rate was fixed at 8 kHz. In the following tests, the noise input was a pure tone sinusoid. For convenience, the reference signal was taken from the same signal generator as the noise signal. In practice, the reference signal could be measured directly from the exciting machinery or synthesized from information related to machinery shaft speed.

The output of the error sensor can be modeled at the nth time step as follows:

$$e(n) = d(n) + \sum_{j=0}^{N-1} P_j \sum_{i=0}^{N-1} w_i(n - j)x(n - j - i) \quad (1)$$

where $d(n)$ is the output at the nth time step due to the primary or noise source above, $x(n)$ the input reference signal, w_i the ith coefficient of the adaptive FIR filter, and P_j the jth coefficient of the transfer function between the output of the adaptive filter and the error sensor. N is the number of filter coefficients. It can be shown that a sinusoidal signal can be arbitrarily modified in magnitude and phase by using a FIR filter with two coefficients. For the following experiments, the value of N was set to 2, thus limiting the controller to narrow band.

The LMS algorithm mean square error signal is defined as follows:

$$J = E[e^2(n)] \quad (2)$$

where E is the expectation operator. This error function is quadratic and, thus, has a unique minimum solution.

At each time step n, the output of the compensating filter $\hat{P}$ was used by the LMS algorithm to minimize J by individually updating each of the adaptive filter coefficients according to the following relation:

$$w_i(n + 1) = w_i(n) - \mu e(n)r(n - i) \quad (3)$$

where

$$r(n - i) = \sum_{j=0}^{N-1} \hat{P}_j x(n - i - j) \quad (4)$$

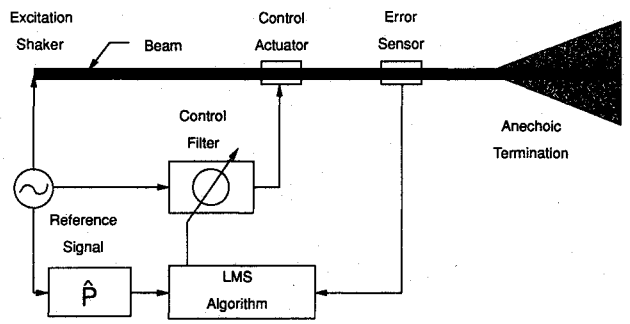

Fig. 3 Control block diagram.

The $r(n)$ is the output of the compensating filter $\hat{P}$. The coefficients of $\hat{P}$ are measured prior to starting the control algorithm. This compensating filter is necessary because the LMS algorithm assumes that the error signal $e(n)$ is the instantaneous result of the control input for which $r(n)$ is a better estimate than $x(n)$. The factor μ of Eq. (3) is a stability parameter that controls the rate of convergence.

Note that the instantaneous error function $e(n)$ is taken as an estimate of the expected value of $e(n)$, and convergence is found to occur in the mean. As shown in Eq. (2), the adaptive LMS algorithm uses a cost function that is based on the mean square amplitude of the error signal. Thus, as the error signal is proportional to bending strain, the control cost function can be seen to be related to an energy variable in the beam. In particular, if the beam is semi-infinite, as in this case, with little reflection of power, then the cost function is directly proportional to flexural power flow.

Experimental Procedure

For the experiment, two different beam arrangements were tested. For the first arrangement, the beam was in a semi-infinite setup. The second arrangement involved the addition of a blocking mass (0.388 or 1.48 kg) located 0.8 m from the free end to provide a finite section of the beam. In this case, the blocking mass causes a discontinuity on the beam that leads to reflection of waves and associated modal response. However, the discontinuity impedance that the beam sees is complex and waves (and, thus, flexural power flow) are transmitted through it. The arrangement thus approximates a beam section joining to, for example, a more complex structure. Rather than reducing the vibration in the finite beam section, we are interested in trying to reduce the power flow leaving the beam at the discontinuity, thus controlling it before it spreads into the more complex supporting structure.

For the semi-infinite case, frequencies of 302 and 802 Hz were tested. For the baseline response, no control was exercised over the primary excitation. Using the Dantec laser vibrometer, out-of-plane velocity vs position was measured every 1 cm along the beam. Control was then applied to the system, and the axial velocity distribution was measured to compare to the no-control case.

For the second test case, blocking mass 1 (0.388 kg) was attached at a position 0.8 m from the free end. The blocking masses have properties given in Table 1 and were clamped symmetrically on each side of the beam by bolts. Because the wavelength of the motion is long compared to their width, they were thought to be representative of line constraints. However, later results show some evidence of wave conversion phenomena suggesting they may also have some distributed characteristics. Frequencies of 412 and 802 Hz were tested. Again, a baseline response was tested for both frequencies with no control over the primary excitation. The laser vibrometer was used to measure the axial velocity distribution. Then, control was applied, and the axial velocity distribution was measured.

Table 1 Blocking mass properties

Blocking mass	Length, m	Width, m	Thickness, m	Young's modulus, GPa	Density, kg/m³	Mass, kg
1	0.0256	0.102	0.055	71.1	2700	0.388
2	0.0512	0.102	0.105	71.1	2700	1.48

Next, blocking mass 2 (1.48 kg) was attached 0.8 m from the free end. A single frequency case of 484 Hz was tested for this arrangement. Another baseline result was obtained to compare to the controlled condition. The control system was activated, and the axial velocity distribution was measured to compare to the no-control case. In addition, a force transducer was inserted in line with the primary shaker. The force transducer output was used in conjunction with the velocity measurement at the drive point to determine the characteristics of the input impedance under the different test cases.

Results

Semi-Infinite Beam

The out-of-plane velocity for the semi-infinite 302-Hz test case is shown in Fig. 4. As mentioned previously, the primary shaker was located at the free end (0.0 m). The control piezoceramics were located at 0.4 m from the free end, and the error sensor piezoceramics were located at 2.15 m.

From Fig. 4, it appears from the no-control case that the termination is ineffective at this frequency. However, calculation of the amplitude reflection coefficient from the standing wave ratio[10] provides an amplitude reflection coefficient of approximately 0.2 and, thus, a power reflection coefficient of <0.05. Thus, in terms of power, the termination performs quite effectively.

When control is applied to the beam, the velocity between the controller and the termination is attenuated on the order of 35 dB. Between the free end and the controller location, the magnitude of the velocity does not change significantly; however, there is significant increase in its standing wave component.

Figure 5 shows the power flow distribution for the 302-Hz test case as calculated from the aforementioned velocity magnitude and phase information (as discussed in the Appendix). The power flows discussed in this paper are referenced to 10^{-12} W. The power flow calculation is accurate except in the proximity of discontinuities on the beam where bending wave near fields are generated. When control is applied, the power flow between the primary source and the controller drops about 20 dB. The controller forces the input impedance that the primary shaker sees to become very reactive, causing real input power flow to drop. Table 2 shows the real and imaginary portion of the input impedance that the primary shaker sees, which was determined as mentioned previously with a force transducer mounted in line with the shaker and the velocity at the drive point. As can also be seen in Fig. 5, the power flow measured between the controller and the error sensor drops an additional 20 dB. This behavior is attributed to the absorption of energy by the controller.

Table 2 Shaker input impedance, semi-infinite beam

Frequency, Hz	Input impedance, N-s/m			
	No control		Control	
	Real	Imaginary	Real	Imaginary
302	2.32	8.47	0.26	9.28
802	2.78	20.15	1.09	16.91

Thus, the control actuator in this configuration can be seen to provide downstream attenuation of flexural power flow by two main mechanisms. First, it creates a largely reactive discontinuity that reflects waves back toward the source, leading to increasing standing wave response and causing the resistive input impedance to fall with an associated drop in input power. Second, it appears to absorb some energy; thus, it acts like a dissipative element. Of course by including either of these variables in the cost function definition one may have some degree of choice over the way the control actuator attenuates downstream energy. Note also that the performance of the controller is unaffected by the standing wave in the noise distribution on the beam. As long as the error sensor is located downstream of the control actuator, the beam motion is attenuated past the control actuator whether the termination is anechoic or not. The result also highlights an advantage of using a piezoceramic element as a sensor. Being distributed, it is less affected by nodes than point sensors. Previous testing has found, for example, that accelerometers are very sensitive to nodal lines giving error signals that flip 180 deg in phase leading to control instabilities.

The flexural velocity distribution for the 802-Hz test case is shown in Fig. 6. Although the termination is more anechoic at this frequency than the 302-Hz case, there is still a small standing wave present on the no-control curve. When control is applied, the velocity between the controller and the error sensor drops from about 4 mm/s to about 0.05 mm/s providing an attenuation of the order of 38 dB. Also, it is noted that the flexural velocity between the controller and the primary

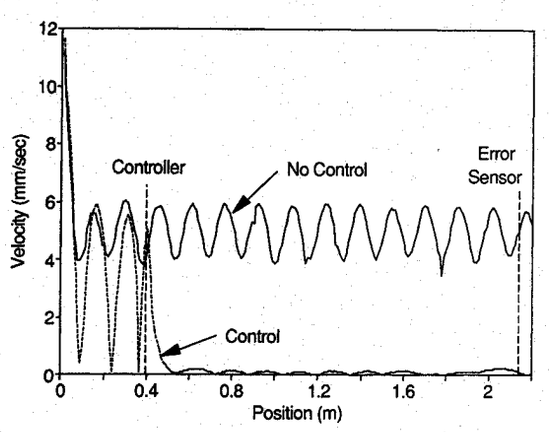

Fig. 4 Flexural velocity distribution, 302 Hz, semi-infinite beam.

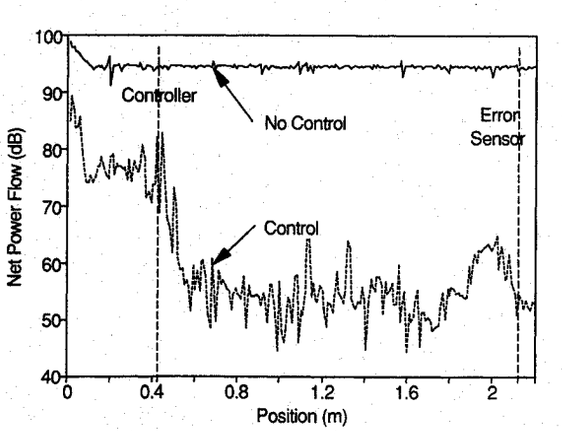

Fig. 5 Power flow distribution, 302 Hz, semi-infinite beam.

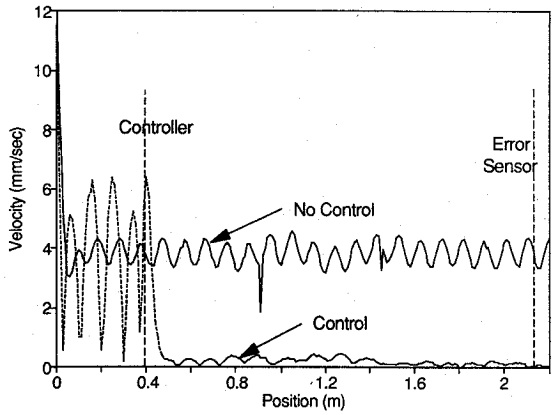

Fig. 6 Flexural velocity distribution, 802 Hz, semi-infinite beam.

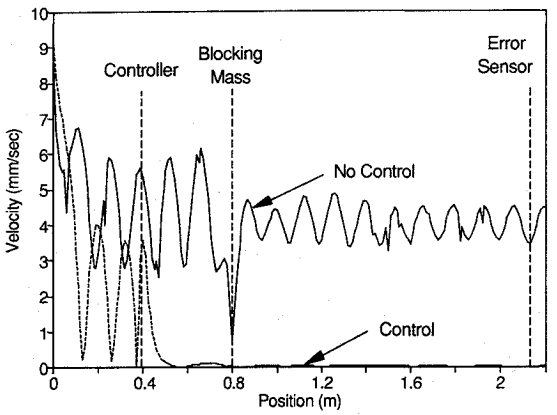

Fig. 8 Flexural velocity distribution, 412 Hz, blocking mass 1.

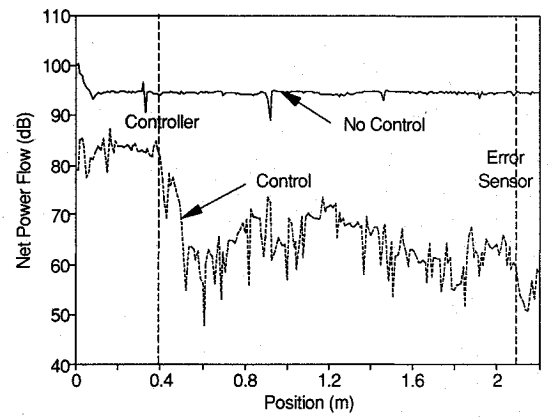

Fig. 7 Power flow distribution, 802 Hz, semi-infinite beam.

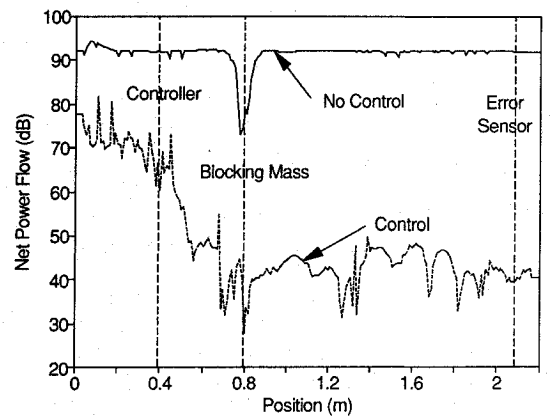

Fig. 9 Power flow distribution, 412 Hz, blocking mass 1.

shaker actually increases in this case when control is applied. The increase in response of the beam section between the controller and the free end was thought to be due to this section being near to resonance with this test frequency and controller input.

The power flow distribution for the 802-Hz semi-infinite case is presented in Fig. 7. When control is applied, the power flow between the primary shaker and the controller decreases about 15 dB because the primary shaker input impedance becomes more reactive, as can be seen in Table 2. The power flow between the controller and the error sensor drops an additional 20 dB due to the absorption of energy by the controller. Overall, the active control provides a 30-dB reduction in power flow at the error sensors. The sharp dips in the power flow distribution were thought to be due to dropouts in the laser vibrometer system, which become more apparent when the out-of-plane response is small (i.e., under controlled conditions).

Finite Beams

The remaining results are with the beam configured with the blocking masses installed. The velocity distribution for the 412-Hz case and blocking mass 1 is shown in Fig. 8.

The blocking mass is located at 0.8 m from the free end, as can be seen by the relatively low velocity at that point on the no-control curve. With no control, a larger standing wave is present between the primary shaker and the blocking mass due to the presence of the blocking mass discontinuity. When control is applied, the velocity between the controller and the error sensor is attenuated on the order of 35 dB, showing the effectiveness of the controller. The velocity of the beam between the primary shaker and the controller also drops. The controller imparts a boundary condition on the system that causes the finite portion of the beam to have a lower response. This result was thought to be due to the fact that the finite section of the beam is being driven off resonance. Similar results have been observed in theoretical calculations using point force actuators.[4]

The power flow distribution for the 412-Hz case is shown in Fig. 9. Table 3 presents the real and imaginary portion of the input impedance at the noise input point. As seen in previous results, the power flow is reduced about 15 dB between the primary shaker and the controller because the primary shaker input impedance becomes more reactive (see Table 3). The power flow between the controller and the error sensor is reduced an additional 20 dB due to the controller absorption of energy. Finally, the power flow between the controller and the error sensor is reduced a total of about 35 dB. The overall reduction in power flow at the error sensor was measured to be >50 dB.

Note that the power flow distribution shows a large dip at the blocking mass location. This is due to the fact that, as discussed in the Appendix, the power flow equations are based on a second-order beam equation and, thus, do not include bending near fields. The results in Fig. 9 thus imply that there are significant near fields generated by the blocking mass.

It is also apparent that the power flow is attenuated immediately after the control actuator, even though the error sensor is located out of the finite section of the beam. This result highlights the observation that if a power-based cost

Table 3 Shaker input impedance, blocking mass 1

Frequency, Hz	Input impedance, N-s/m			
	No control		Control	
	Real	Imaginary	Real	Imaginary
412	46.0	266	3.66	235
802	2.78	17.3	1.58	18.2

function is used then control of the beam can be achieved with a single actuator.

The velocity distribution for the 802-Hz case is presented in Fig. 10. For the no-control case, the standing wave between the primary shaker and the blocking mass is larger than previous cases because 802 Hz appears to be near a resonance of the finite portion of the beam. When control is applied (two-sided error sensor), the velocity between the blocking mass and the error sensor is attenuated on the order of 35 dB. The velocity distribution can also be seen to be markedly reduced past the control actuator, leading to a global reduction in beam response with one actuator. The other curve presented in Fig. 10 corresponds to the use of a single-sided error sensor for control. Since a single-sided error sensor can sense both extensional and flexural waves, the comparatively poor reduction was attributed to the controller seeking the minimum of the superposition of the two waveforms at the error sensor. The minimum in this case does not correspond to the minimum of pure flexural waves, and, thus, the use of a two-sided error sensor more effectively controlled the flexural wave.

The power flow distribution for the 802-Hz case is shown in Fig. 11. As noted previously the controller reduces the power flow at the error sensor by two methods. First, the controller forces the input impedance that the primary shaker sees to be more reactive, which reduces the power flow into the beam by about 10 dB. Second, the controller absorbs an additional 10 dB. The net power flow at the error sensor is reduced about 40 dB.

It is also interesting to note the drop in power flow across the blocking mass for the no-control case. If there is conservation of energy on the beam and there is only flexural motion, then these values should be the same as the power flow technique measures net power flow. It was thought that a wave conversion phenomena was occurring at the blocking mass discontinuity. Because of the distributed nature of the blocking mass, flexural waves were thought to be coupling into extensional waves on the beam at the mass discontinuity location. Wave conversion behavior at blocking masses and discontinuities on beams have been previously observed.[11] Work discussed in Ref. 12 reveals that there is both flexural and extensional waves present on the beam past the blocking mass. As these waves are largely unobservable by the laser vibrometer and can carry high power (due to the beam being stiffer in extension), the measured power flow falls by around 20 dB.

Figure 12 presents the velocity distribution at 484 Hz with blocking mass 2 located at 0.8 m. As seen in the figure, there is a significant standing wave present on the beam between the primary shaker and the blocking mass for the no-control case that is due to the size of the blocking mass (1.48 kg). When control is applied, the velocity downstream of the controller is attenuated about 20 dB, but the response between the controller and the primary shaker increases.

The power flow distribution for the 484-Hz test case is presented in Fig. 13. There are several interesting characteristics apparent in the results. For the no-control case, the power flow drops substantially past the blocking mass location. Blocking mass 2 is physically larger than blocking mass 1 and, thus, is more distributed in nature. This increase in size and mass is thought to be the reason for the significant wave conversion at the blocking mass and subsequent drop in flexural power flow.

Figure 13 also shows that the net power flow input into the beam does not change significantly when control is applied. However, there is a large drop in power flow after the controller location and, thus, most of the attenuation of energy at the error sensor appears to be due to the controller piezoceramic element absorbing vibrational power. These observations are confirmed by the input impedance for which

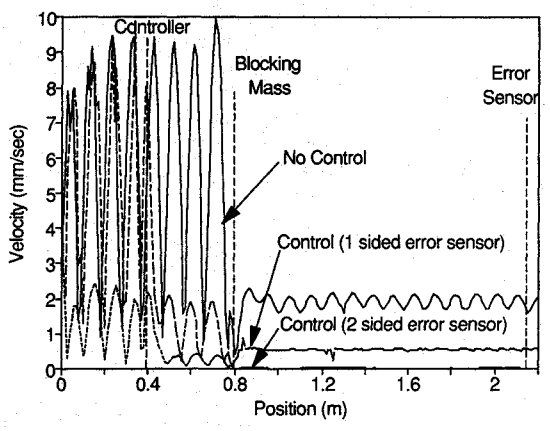

Fig. 10 Flexural velocity distribution, 802 Hz, blocking mass 1.

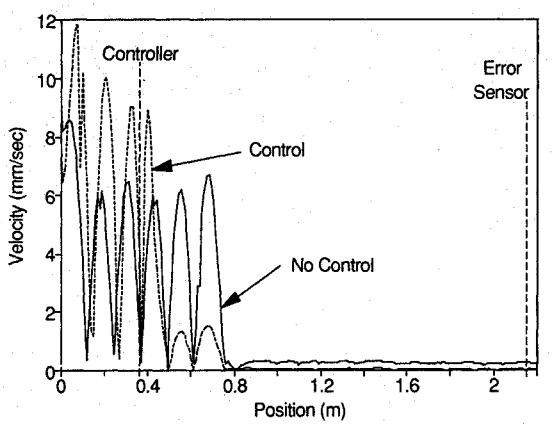

Fig. 12 Flexural velocity distribution, 484 Hz, blocking mass 2.

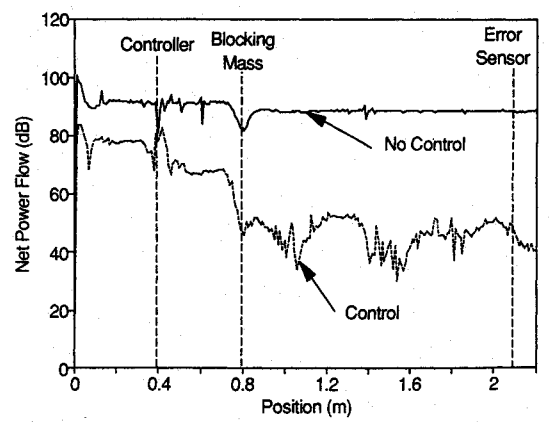

Fig. 11 Power flow distribution, 802 Hz, blocking mass 1.

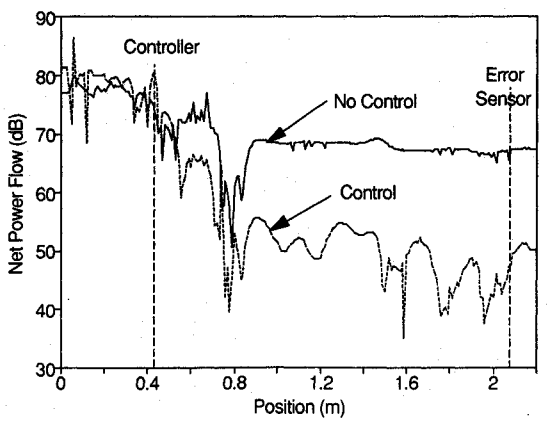

Fig. 13 Power flow distribution, 484 Hz, blocking mass 2.

little change of the resistive component is observed for this control case.

Extensional waves were also found to be present on the error sensors. Figure 10 shows the velocity distribution of the beam driven at 802 Hz with blocking mass 1 on the beam for three different situations. When a single error sensor element was used on one side of the beam (one-sided error sensor), while the error signal was attenuated by 40 dB, the laser vibrometer showed attenuations of only on the order of 10 dB. This result was again thought to be due to the presence of extensional waves interfering with the strain signal of the flexural waves on the piezoceramics. This problem was cured by using two piezoceramic elements in symmetric pairs with their signals summed 180 deg out of phase (two-sided error sensor), as shown in Fig. 10. In other work,[12] simultaneous control of flexural and extensional waves is demonstrated by letting the symmetric elements of the actuator and sensor be floating transducers of a two-channel adaptive controller.

Concluding Discussion

The active control of flexural vibrations and power flow has been experimentally studied. In particular, piezoceramic transducers that are bonded symmetrically on each side of the beam and used in conjunction with an adaptive LMS controller have demonstrated attenuations in flexural power flow and vibrations in both semi-infinite and finite beams on the order of 30 dB or more. The approach has also been demonstrated to be robust with high attenuations obtained over a wide range of frequencies and differing beam configurations. Different mechanisms of control have been shown.

In conjunction with the control experiments, the use of a laser vibrometer as a noncontacting sensor to measure beam out-of-phase velocity and, more important, flexural power flow has been demonstrated. This device shows much potential for research in structural energy flows.

The work clearly shows that piezoceramic elements have much potential for active/adaptive control of power flow in structures. These elements have both size and weight advantages over conventional transducers and, in conjunction with multichannel controllers, are a step toward the creation of highly integrated distributed control systems.

Future work will concentrate on the simultaneous control and measurement of flexural and extensional power flow. Additional work will also focus on increasing the authority of the actuators.

Appendix: Measurement of Structural Power Flow Using a Laser Vibrometer

Past work relies on determining flexural power flow using signals from surface-mounted accelerometers.[13] However, this approach suffers from a number of disadvantages, among which are added mass to the structure, inadequacy of location, sensitivity to rotation, and phase calibration errors.

In this paper, the flexural power flow was estimated using a Dantec laser vibrometer, which when scanned axially along the beam, provided measurements of the beam out-of-plane velocity and phase, without the problems just listed.

For the work considered here, only propagating flexural waves were considered; bending near fields generated at discontinuities was assumed to be decayed to zero.

The beam equation can thus be written in reduced form as

$$\frac{d^2\bar{y}}{dx^2} + k_f^2\bar{y} = 0 \tag{A1}$$

where $y(k)$ is the spectral content of the beam transverse response and the flexural wave number:

$$k_f = \left(\frac{m'\omega^2}{EI}\right)^{1/4} \tag{A2}$$

where m' is the mass per unit length, ω the frequency of excitation, and EI the bending rigidity term. The power flow is the time-averaged sum of the shear and bending moment components, as follows:

$$P = <Q\dot{y}>_t + <M\dot{\theta}>_t \tag{A3}$$

The moment is related to the axial displacement using the following relation:

$$M = EI\frac{d^2y}{dx^2} \approx EIk_f^2 y \tag{A4}$$

Under free-field conditions, the total power flow is shared equally by the shear and bending components. Thus, Eqs. (A3) and (A4) can be combined and reduced to

$$P = 2EIk_f^2 <y\dot{\theta}>_t \tag{A5}$$

The following finite difference approximations allow the displacement and rotational velocity to be approximated:

$$y \approx [y_1 + y_2]/2 \tag{A6a}$$

$$\theta \approx [\dot{y}_1 - \dot{y}_2]/2 \tag{A6b}$$

Substituting the finite difference relations, Eqs. (A6) into Eq. (A5), the result is

$$P = \frac{EIk_f^2}{\Delta_x}[<y_1\dot{y}_1>_t + <y_2\dot{y}_1>_t - <y_1\dot{y}_2>_t - <y_2\dot{y}_2>_t] \tag{A7}$$

If Eq. (A7) is written in terms of acceleration instead of displacement and velocity and the Fourier transform is taken, the resulting power flow is

$$P(\omega) = -\frac{2EIk_f^2}{\Delta x\omega^3}\,\mathrm{Im}(S_{21}) \tag{A8}$$

where S_{21} is the cross spectrum between the accelerometer response at two points on the beam, and Δx is the spacing of the points.

In order to process the velocity information of the laser vibrometer, Eq. (A3) can be rewritten as

$$P(\omega) = \frac{2EIk_f^2}{\Delta x\omega}\,\mathrm{Im}(S'_{21}) \tag{A9}$$

where S'_{21} is the cross spectrum of the velocity response.

In the actual experimental setup, the Dantec laser vibrometer was interfaced to a B&K spectral analyzer. The scanning drive and the B&K analyzer were controlled by an IBM AT computer, which determined and calculated cross-spectral information. The step size of measurement points Δx was determined by calculating the flexural wave number from Eq. (A2). The spacing was set equal to a quarter wavelength.

Acknowledgments

This work was funded by Grant NAG 1-390 from the Structural Acoustics Branch of NASA Langley Research Center. The authors are grateful to Richard Silcox and Don Brown of NASA Langley for help with the laser vibrometer and the control algorithm.

References

[1]Redman-White, W., Nelson, P. A., and Curtis, A. R. D., "Experiments on Active Control of Flexural Wave Power," *Journal of*

Sound and Vibration, Vol. 112, No. 1, 1987, pp. 187–191.

[2]Von Flotow, A H., and Schafer, B., "Wave Absorbing Controller for a Flexible System," *Journal of Guidance, Control, and Dynamics*, Vol. 9, July–Aug. 1986, pp. 673–680.

[3]Gonidou, L. O., and Fuller, C. R., "Further Research on Active Control of Flexural Power Flow in Elastic Thin Beams," *Journal of the Acoustical Society of America*, 85(S1), 1989, p. 573.

[4]Gonidou, L.-O., "Active Control of Flexural Power Flow in Elastic Thin Beams," M.S. Thesis, Virginia Polytechnic Inst. and State Univ., Blacksburg, VA, Feb. 1989.

[5]Meirovitch, L., and Norris, M. A., "Vibration Control," *Proceedings of Inter-Noise 84*, Noise Control Foundation, New York, 1984, pp. 477–482.

[6]Crawley, E. F., and deLuis, J., "Use of Piezoelectric Actuators as Elements of Intelligent Structures," *AIAA Journal*, Vol. 25, No. 10, 1987, pp. 1373–1385.

[7]Pines, D. J., and von Flotow, A. H., "Active Control of Bending Wave Propagation at Acoustic Frequencies," *Proceedings of American Control Conference*, Institute of Electrical and Electronics Engineers, 1989, pp. 221–229.

[8]Gibbs, G. P., and Fuller, C. R., "Active Control of Flexural Power Flow in Beams Using Piezoceramic Actuators," *Journal of the Acoustical Society of America*, 86(HH6), 1989, p. 584.

[9]Widrow, B., and Sterns, D., *Adaptive Signal Processing*, Prentice-Hall, Englewood Cliffs, NJ, 1985.

[10]Morse, P. M., and Ingard, K. U., *Theoretical Acoustics*, Princeton University Press, Princeton, NJ, 1968.

[11]Cremer, L., Heckel, M., and Ungar, E., *Structure-Borne Sound*, Springer-Verlag, Berlin, 1973.

[12]Fuller, C. R., Gibbs, G. P., and Silcox, R. J., "Simultaneous Active Control of Flexural and Extensional Power Flow in Beams," *Journal of Intelligent Material Systems and Structures*, Vol. 1, No. 2, 1990, pp. 235–247.

[13]Downing, J. M., and Shepard, K. P., "Power Flow in Beams Using a 5-Accelerometer Probe," *Proceedings of Noise-Con 88*, Noise Control Foundation, New York, 1988, pp. 335–340.